Available online at www.sciencedirect.com
ScienceDirect
International Journal of Multiphase Flow 33 (2007) 904–920
International Journal of Multiphase Flow
www.elsevier.com/locate/ijmulflow

Effect of ambient pressure on penetration of a diesel spray

I.V. Roisman *, Lucio Araneo [1], C. Tropea

Darmstadt University of Technology, Chair of Fluid Mechanics and Aerodynamics, Petersenstr. 30, 64287 Darmstadt, Germany

Received 17 July 2006; received in revised form 22 January 2007

Abstract

In the present experimental and theoretical work the propagation of a high-speed fuel spray at distances much longer than the breakup length is studied. The motion of the spray is modeled in two regions: the *main region* of the steady flow and the *front region* of the spray. The analysis yields the equation of propagation of the tip of the spray. These theoretical results have been validated against experimental data obtained from a common-rail diesel injection nozzle and from other data available in the literature. The importance of the shock wave propagation at the initial stage of the spray injection is demonstrated.

Keywords: Spray; Spray penetration; Fuel injection; Ambient pressure

1. Introduction

Experimental investigation and modeling of fuel spray are extremely challenging problems. The spray, especially in the neighborhood of the nozzle, is very dense, making the use of conventional optical measurement techniques (such as the phase Doppler technique or PIV) very difficult. This is the reason why spray penetration and cone-angle, which can both be obtained using photographic techniques, are among the most frequently reported parameters in fuel-spray research. Such a technique has been used in one of the first experimental studies (Miller and Beardsley, 1926) on the effect of the ambient pressure (or in fact the density of the ambient gas) on the penetration length of an engine spray.

There are several models, semi-empirical or numerical, of spray penetration. In these studies (Wan and Peters, 1999; Sazhin et al., 2001; Naber and Siebers, 1996) the penetration of a spray was calculated by solving the cross-sectionally averaged equations of the flow, describing the mass and the momentum balance in the spray. The conditions at the front edge of the spray have not yet been considered for dense sprays.

Experimental observations of spray penetration under high-ambient pressure conditions show that near the spray tip vortex-ring-like structures are frequently developed. Such structures have been observed in most of

* Corresponding author. Tel.: +49 6151 163 554.
E-mail address: roisman@sla.tu-darmstadt.de (I.V. Roisman).
[1] Present address: Politecnico di Milano, Dipartimento di Energetica, via La Masa 34, Milano, Italy.

0301-9322/$ - see front matter
doi:10.1016/j.ijmultiphaseflow.2007.01.004

the experimental studies of fuel spray injection, e.g. Cao et al. (2000), di Stasio et al. (2000) and Stegemann et al. (2002).

Similar mushroom-like shapes have been observed in galaxy "worms" of the length of the order of 1000 light years (English et al., 1999), in streams generated during volcano eruptions, and in experiments associated with penetration mechanics, where metal rods or shaped-charge jets move with the velocity of order of 10^3 m/s. Hydrodynamic models of the type considered in Birkhof et al. (1948), Sagomonyan (1974) and Roisman et al. (2001) take into account the erosion of the projectiles and deformation of the shaped-charge jets near the front edge and allow one to successfully predict their penetration.

An attempt to understand and to describe the conditions at the tip region of the spray was made by Sjöberg (2001). The main assumption of his model is that the drops are collected in a region near the spray tip. In this spray penetration model the shape of the near-tip region is approximated by a ball of growing radius.

The main subject of the present paper is the experimental investigation and the modeling of a Diesel spray. Our study is focused on the modeling of the ambient pressure influence on the temporal evolution of the spray length.

Any theoretical model can be assumed reliable if it is confirmed by an experimental evidence and (what is not less important) if it has no internal contradictions. The aim of the present model is to identify and to incorporate the "main players" in terms of forces governing the phenomena. It is well-known that the spray penetration depends, among other parameters, on the geometry of the nozzle and on the details of the internal flow. These factors have never been incorporated into breakup or penetration models. Therefore, any spray penetration model (including the proposed one) should have at least one adjustable parameter accounting for the nozzle geometry. In our model this parameter is the breakup length R_0, which will be defined more precisely below. This quantity is determined by fitting of the predictions to experimental data. The main difference between our model and the previous models is that two important features typical for high-speed, dense Diesel sprays injected into a high-pressure chamber are accounted for. The first feature is the specific kinematic and dynamic conditions at the front edge of the spray where the volume fraction of the liquid jumps dramatically over a very short length. The second feature is that at high-injection pressures the injection velocity can be comparable with the sound speed in the air; hence compressibility effects have to be accounted for. These two features lie in the focus of the proposed study.

Our hydrodynamic model describing the penetration of a dense fuel takes into account the inertia of the ambient gas and the jump conditions near the leading edge of the propagating spray. It is assumed that the evaporation of droplets in the spray does not influence the total momentum of the penetrating spray, and its effect is not considered in the present study. This assumption is supported by the results of Wan and Peters (1999) and by the numerical study of spray propagation by Iyer et al. (2001).

2. Theoretical model of far-field spray penetration

In the present model it is assumed that the front of the penetrating spray is so far from the nozzle that the details of the flow near the nozzle, determined by its geometry, do not influence the penetration process. In this chapter a simplified model for the spray velocity and volume fraction distribution is developed accounting for the inertia of the spray and entrained air. Next, the jump conditions at the tip of the spray are considered yielding the equations of motion of the spray.

Consider the spray propagating in the ambient air. In the present model the spray is subdivided into two main regions (see Fig. 1). The region ① is far from the front edge of the spray. The flow here is assumed to be steady; the pressure gradient is negligibly small. At the leading edge of the spray the droplets collect in the front region ②. The details of the jet breakup near the nozzle ($r < R_0$) are not discussed in the present model. The model for spray penetration is valid for the distances much larger than R_0.

The concentration of drops in the dense Diesel spray is very high. Therefore, it is doubtful whether a description of the motion of a single drop in air can be helpful or applicable to the prediction of the spray propagation. The mass fraction of the liquid phase in such sprays significantly exceeds the mass fraction of the air. The momentum of the gas fraction is therefore negligibly small compared to the momentum of the liquid fraction. Therefore, we can expect that the velocity of the gas approaches the average drop velocity very quickly. Hence the velocity of the surrounding gas can be approximated by the local average velocity of the

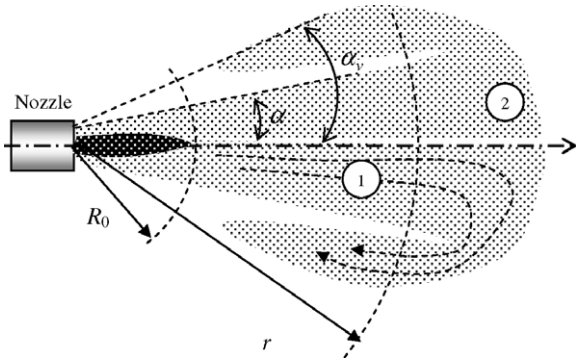

Fig. 1. Sketch of the propagating spray. (1) corresponds to the region of the steady radial expansion, (2) is the spray compressed in the front region.

drops in the spray. This assumption is supported by the results of the study of Liu et al. (1993), showing that the spray penetration predicted by the model is virtually not influenced by the drag model. Actually, the present asymptotic model corresponds to the limiting case of the drag coefficient approaching infinity, thus equating the velocities of the liquid and gaseous phases in the spray. The existence of a large zone in the spray far from the nozzle where the induced gas velocity is comparable with the droplet velocity was also mentioned in Ghosh and Hunt (1994). In the following analysis we neglect velocity differences of the gas and liquid phases in a zone near the nozzle, assuming this zone to be much shorter than the penetration length.

2.1. Steady flow in the region of the steady radial expansion

Consider the steady-state flow of the spray in the region (1) far behind the front of the spray (the injection is assumed to be steady). Consider a spherical coordinate system with the origin at the nozzle region. We assume that at the distances much larger than the nozzle diameter the spray propagates radially with the velocity $u(r)$, where r is the radial coordinate defined in Fig. 1. This strong assumption is confirmed by wide variety of experimental studies of the spray propagation showing an almost conical shape of the spray with the constant half-angle in the steady region (1).

It should be emphasized that we do not describe the details of the flow in the region (1). In the present quasi-one-dimensional model a kinematically admissible flow is assumed which satisfies the mass and momentum balance in the spray. This flow is used to estimate the conditions at the front edge of the spray and to obtain equations of its motion.

Such kind of approximations of the flow in the region (1) are rather conventional. See for example the integral model for spray propagation by Cossali (2001); the theoretical model of Desantes et al. (2006) assuming the Gaussian velocity profile in the spray; or the theoretical model of Pozorski et al. (2002) accounting for the gas turbulence. The main interest of the present study is the study of the influence of the edge of the spray. Therefore, for the description of the flow in the region (1) we have chosen the simplest possible but still reliable quasi-one-dimensional model described below.

The total mass conservation of the liquid phase and the momentum balance of the mixture in the radial direction lead to:

$$\frac{\partial}{\partial r}[r^2\gamma(r)u(r)] = 0, \tag{1a}$$

$$\frac{\partial}{\partial r}[\rho r^2\gamma(r)u(r)^2 + \rho_a r^2(1-\gamma(r))u(r)^2] = 0, \tag{1b}$$

where γ is the volume fraction of the liquid phase, $u(r)$ is the radial velocity of the mixture, ρ and ρ_a are the densities of the liquid and air. Here the momentum of the air flow in the azimuthal direction is assumed to be negligibly small and the pressure is thus assumed to be constant. The effect of the drops evaporation is also neglected in the present model.

The solution of the above equations is

$$\gamma = \frac{C_1}{2r^2}A(r), \quad u = \frac{C_1 C_2 \Delta\rho}{A(r)}, \quad A(r) = C_1\Delta\rho + \sqrt{C_1^2\Delta\rho^2 + 4r^2\rho_a}, \tag{2a, b, c}$$

where $\Delta\rho = \rho - \rho_a$, and the integration constants C_1 and C_2 are given by

$$C_1 = \frac{\gamma_0 R_0}{\sqrt{\gamma_0\Delta\rho + \rho_a}}, \qquad C_2 = 2U_0\left(1 + \frac{\rho_a}{\gamma_0\Delta\rho}\right). \tag{3a, b}$$

The radius R_0 corresponds to the radial coordinate of the breakup of the injected jet. At this position the drop velocity is U_0 and $\gamma = \gamma_0$. This radius depends on the geometry of the nozzle, on the density of the gas and of the fuel, and on the deformation of the jet.

Consider now the cross-section of our conical spray region by a sphere of the radius r centered at the cone top. The cross-sectional area S is

$$S = 2\pi r^2(1 - \cos\alpha), \tag{4}$$

where α is the half-angle of the cone. The total volumetric flow rate of the spray liquid phase through the cross-section of radius r is $Q = Su\gamma$. At the breakup radius this flow rate is expressed using (4) as $Q = 2\pi R_0^2(1 - \cos\alpha)U_0\gamma_0$. On the other hand, in the assumed steady state this flow rate is equal to the flow rate of the liquid injected through the nozzle, $Q = \pi D_{\text{Nozzle}}^2 U_i/4$. Next, noting the high Weber number of the drops as discussed in the previous section, the energy lost due to the creation of the droplets' surface is small in comparison with the kinetic energy and the initial droplet velocity can be well approximated by the injection velocity: $U_i = U_0$. With the help of Eqs. (2)–(4) the volume balance of the spray yields the following expression for the breakup radius R_0:

$$R_0 = \frac{D_{\text{Nozzle}}}{\sqrt{8\gamma_0(1 - \cos\alpha)}}. \tag{5}$$

2.2. Near-nozzle boundary conditions

Although the breakup of the injected jet in this region is very difficult to investigate experimentally, it is generally accepted that liquid filaments are successively removed from a central liquid core in the downstream direction. This suggests that the atomization of the jet can be described using the "chaotic disintegration" approach of Yarin (1993). The volume fraction of the liquid phase reduces with the inverse of the distance squared from the nozzle, $\gamma \sim r^{-2}$, whereas the volume fraction $1 - \gamma$ of the voids increases. Consequently, their size and the number density grow and they begin to merge, leading to fragmentation of the jet. The jet in this intermediate region can be described as a liquid infinite cluster occupying the relative volume γ. In terms of the percolation theory of Staufer (1985), the probability that an elementary particle occupies a liquid site is γ, whereas the probability that it belongs to a lacunae (void) is $1 - \gamma$. At some critical probability, the percolation threshold (Roisman et al., 2001; Yarin, 1993; Staufer, 1985; Staufer, 1979), corresponding to $\gamma^* = 0.311$ in the three-dimensional case, the "infinite" cluster is broken and the distribution of finite clusters (droplets of various diameters) appears. Therefore, the volume fraction $\gamma_0 = \gamma^*$ corresponds to the complete disintegration of the jet and is the maximum possible volume fraction of a liquid phase of a spray consisting of separate droplets.

2.3. Jump conditions at the front edge of the spray

The above analysis is not valid at the front of the spray where the volume fraction of the liquid phase jumps from γ to 0. The resistance of the air leads to a compression of the spray in the front region and leads to the appearance of the vortex-ring-like structures of the spray. The velocity of drops in the relatively thin layer near the front end of the propagating spray is significantly lower than those in the steady region (1). This fact has been confirmed by the measurements of Diesel sprays using the phase Doppler instrument (Araneo and Tropea, 2000).

Here we consider times much longer than the characteristic time of the shock wave, D_{Nozzle}/c, and a spray-tip velocity much smaller then the speed of sound in gas c. Under these conditions the ambient gas can be modeled as incompressible. The gas stagnation pressure at the tip of the spray can be estimated using the Bernoulli equation as $p_a + \rho_a U_T^2/2$. The pressure in the region ① of the spray behind the front region is p_a because the inertia of the gas flow in the azimuthal direction is negligibly small. The momentum equation at the front edge of the spray expresses the balance of the inertia of the liquid and the gas phases of the spray entering the front region with the relative velocity $u - U_T$ and the pressure of the gas at the front region just outside the spray:

$$[\rho\gamma + \rho_a(1-\gamma)](u - U_T)^2 = \frac{\rho_a U_T^2}{2}. \tag{6}$$

The inertia of the flow in the azimuthal direction is assumed to be small in comparison with the inertia in the axial direction and is therefore neglected.

The solution of Eq. (6) for $U_T < u$ is:

$$U_T = u\left[1 + \sqrt{\frac{\rho_a}{2(\rho_a + \Delta\rho\gamma)}}\right]^{-1}. \tag{7}$$

Now the ordinary differential equation for the temporal propagation of the spray tip can be written in the form

$$\frac{\mathrm{d}R_T}{\mathrm{d}t} = U_T. \tag{8}$$

Here R_T is the penetration length.

2.4. Solution for the penetration length

The solution of Eq. (8) can be written in dimensionless form, taking R_0 as a length scale and U_i as a velocity scale. Denoting

$$\varsigma = \frac{\rho_a(\Delta\rho\gamma_0 + \rho_a)}{\Delta\rho^2\gamma_0^2}, \qquad \eta = 2 + \frac{2\rho_a}{\Delta\rho\gamma_0} \tag{9}$$

yields

$$\gamma = \frac{\gamma_0}{\eta\bar{r}^2}\left[1 + \sqrt{1 + 4\bar{r}^2\varsigma}\right], \qquad \bar{u} = \frac{\eta}{1 + \sqrt{1 + 4\bar{r}^2\varsigma}}, \tag{10a, b}$$

$$\bar{U}_T = \frac{\bar{u}}{1 + \left[2 + \frac{4\gamma}{(\eta-2)\gamma_0}\right]^{-1/2}}. \tag{10c}$$

Here and below the overbared variables are dimensionless.

The solution of Eq. (8) for the penetration length after breakup can be written in the following form:

$$\bar{t} - \bar{t}_0 = \int_{\bar{R}_0}^{\bar{R}_T} \frac{1}{\bar{u}(\bar{r})}\left[1 + \left[2 + \frac{4\gamma}{(\eta-2)\gamma_0}\right]^{-1/2}\right]\mathrm{d}\bar{r}, \tag{11}$$

where $\bar{t}_0$ is the time shift associated with the initial jet penetration and breakup.

At relatively long distances ($\varsigma^{1/2}\bar{r} \ll 1$) the approximate solution for the penetration length can be written in the form:

$$\bar{R}_T \approx a + \sqrt{2 - \sqrt{2}}\varsigma^{-1/4}\eta^{1/2}(\bar{t} + \tau)^{1/2}, \tag{12}$$

where a and τ are some dimensionless constants. The above well-known square root dependence of the penetration length with time at long distances was reported in several experimental studies, for example Arai et al. (1984) and Senduka (1998), see also the review Dent (1971) of the models for spray penetration.

3. Experimental set-up and procedure

A common-rail diesel injector with the nozzle of inner diameter $D_{\text{Nozzle}} = 0.190$ mm has been used to study the fuel spray penetration at various injection pressures ($p_i = 300$, 500, 700, 1000 and 1350 bar). The fuel was injected into a pressure chamber, allowing one to vary the air ambient pressure. Spray penetration data were collected for the ambient pressures $p_a = 1$ (atmospheric pressure), 3, 5, 7, 10, 16 and 25 bar. The density of the liquid is 817 kg/m^3. The experimental set-up is shown schematically in Fig. 2. A detailed description of the experimental setup and the results can be found in Kuß (2000) and Araneo and Tropea (2000).

The nozzle diameter is relatively large in comparison with the modern atomizers used to inject Diesel fuel. It is known that the inner diameter of the nozzle and its geometry influence the properties of the injected spray. A larger nozzle diameter increases the linear part of the spray, maintaining it long enough to be easily measured at high ambient pressures. However, the modeling principles are the same for all dense sprays. The experiments performed with this nozzle do not represent the latest injection technology but they are very useful to validate the proposed theoretical model.

The injected spray is visualized using a CCD camera (PCO Sensicam, 1280×1024 pixels) operated with an exposure time of 2 μs and a synchronized stroboscope placed at an off-axis angle of 60°. In Fig. 3 the shape of the spray at various time instants is shown for two different ambient pressures: $p_a = 1$ bar and $p_a = 25$ bar – all other parameters of injection are the same. The photos are inverse images. Therefore the illuminated parts are shown as dark regions. Such images are used to estimate the penetration length of the spray. The time intervals between the exposures have been varied in the range from 0.1 ms to 0.5 ms, depending on the stage of spray penetration and on the penetration velocity.

The pressure chamber is equipped with circular quartz windows allowing a view of nearly 110 mm. The maximum spray length visible at any configuration is limited to approximately 105 mm. With a view of the complete spray from the injector to the spray tip, this is sufficient at 10, 16 and 25 bar to observe the complete injection. The resolution in this case was set at 10 pixels per millimeter.

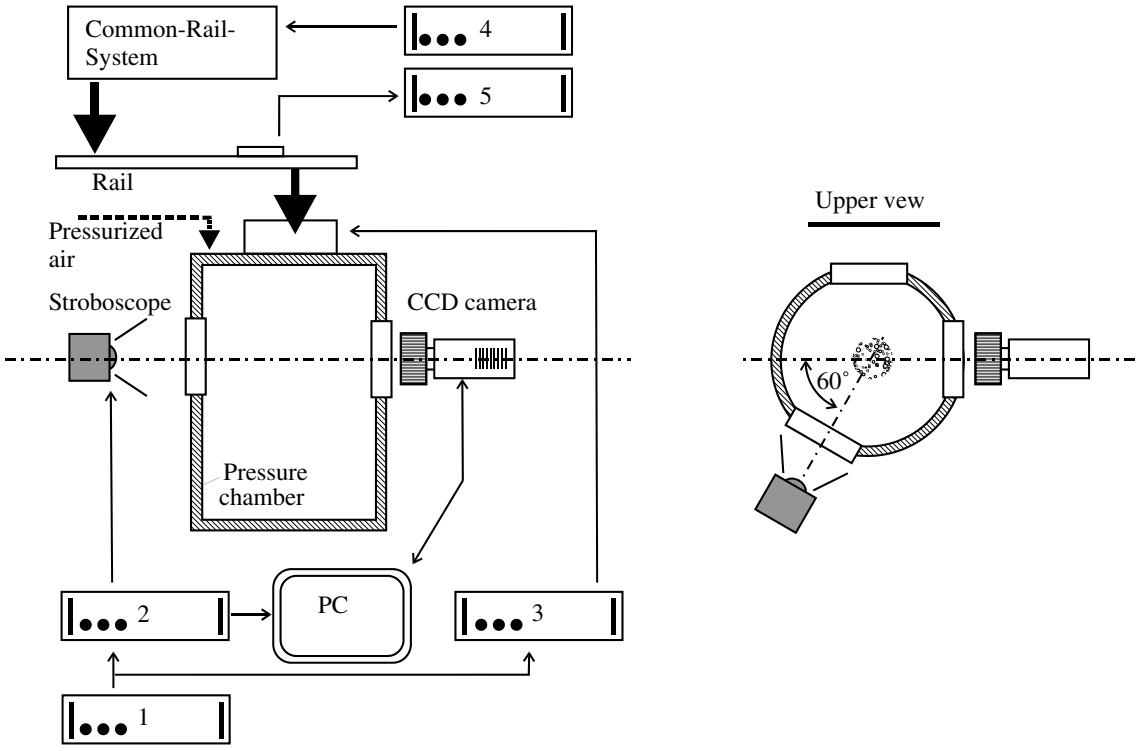

Fig. 2. Scheme of the experimental set-up. The electronic parts are: 1 – signal generator, 2 – signal delayer, 3 – signal generator for the injector, 4 – injector controller, 5 – injection pressure detector.

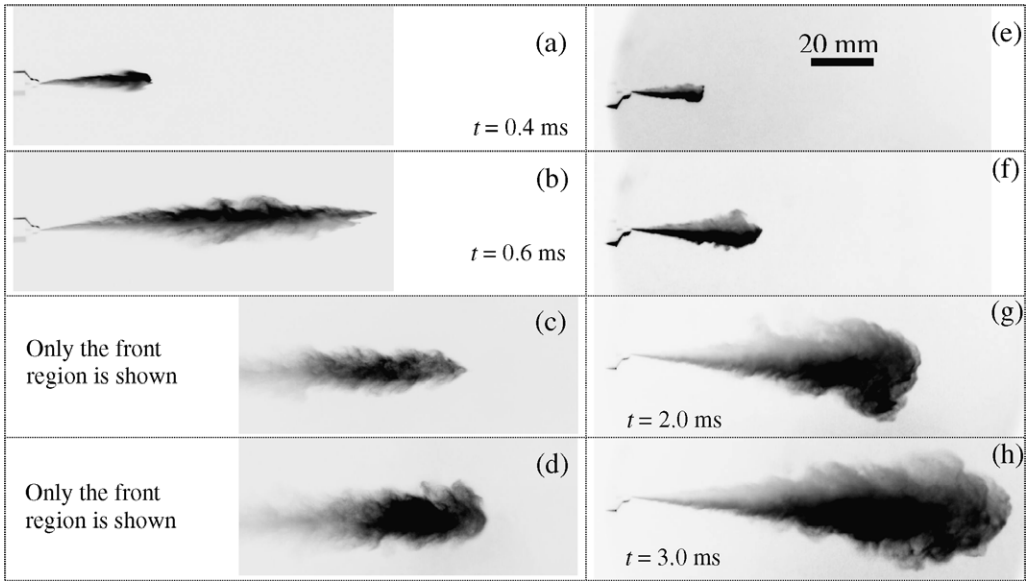

Fig. 3. Shape of the spray at different instants after injection. The ambient pressure is $p_a = 1$ bar (images on the left) and $p_a = 25$ bar (images on the right). The time instants are: (a, e) 0.4 ms; (b, f) 0.6 ms; (c, g) 2.0 ms; (d, h) 3.0 ms.

At intermediate pressure (3, 5 and 7 bar) the penetration length in many cases exceeded the limit of 105 mm. A spacer ring of 40 mm was used to displace the injector upwards. In this configuration the injector is no longer visible. Only the distances from 40 to 140 mm could be observed with the same resolution of 10 pixels per millimeter.

At 1 bar even the 40 mm spacer was too short since the penetration length is much longer than 140 mm. In this case a set-up in open air was used, with a much larger field of view of up to 200 mm, with a corresponding resolution of 6 pixels/mm. By moving the camera to two different positions it was then possible to measure the spray tip position up to 350 mm from the injector. The illumination was directed only towards the spray tip to preserve the image quality of the investigated region.

A much higher resolution (55 pixels per millimeter, with a consequently smaller field of view of few millimeters) was used to visualize correctly the small jet protruding from the spray at the very initial injection stage.

The acquisition of images is not cycle resolved, which means that each image issues from a different injection. To reduce cycle-to-cycle variations, ten images were acquired at each time step. The internal part of the pressure chamber was black painted, to increase the image contrast and enhance the visibility of the spray.

The digital images have been automatically processed using the software Optimas; the spray tip position has been detected by standard digital image analysis routines (back-ground subtraction, object detection).

It is well known that the experimental description of the shape of dispersed medium like a spray using photographic techniques suffers from the inability to detect regions of low concentration of the liquid phase. In fact, the measured values of the spray length can be illumination dependent. The error in such measurements depends on the size of the regions at the spray periphery where the gradient of the concentration is significant. In Fig. 3 it can be clearly seen that the illumination of the spray is not uniform. This is explained by the configuration of the photographic system. However the contours of the spray are almost symmetric. This result indicates that at the edges of the spray the concentration jumps in a relatively thin layer and that the measurements are only slightly influenced by the illumination.

The uncertainty in the length measurements is approximately 2 pixels, corresponding approximately to $\varepsilon_l = 0.2$ mm the most used resolution of 10 pixel/mm. The approximate error of the difference in measurements of the spray lengths at consecutive time steps is of the same order. Therefore, the maximum error is estimating the spray tip velocity is $\varepsilon_l/\varepsilon_t = 0.42$ m/s. The typical measured penetration velocities are much higher than 50 m/s. The relative error is thus approximately 1%.

Most of the experimental results presented in the present paper are obtained with this experimental setup. Some additional experimental data found in the literature have also been used to validate the theoretical model.

4. Results and discussion

It can be seen that the appearance of the vortex-ring-like structures is more pronounced for the case of higher ambient pressures (see Fig. 3(g) and (h)), indicating that the air density at the front edge determines the shape of the cloud of the particles and its penetration.

Note that in the present paper the penetration length is denoted by R_T. This notation is the most convenient, since the theoretical model describes the spray in spherical coordinates.

A typical temporal propagation of the tip of a fuel spray is shown in Fig. 4. Two main stages of penetration can be immediately recognized (Arai et al., 1984). During the first stage the spray tip propagates nearly linearly in time, $R_T \sim t$. The first stage is followed by the second stage in which the length of spray can be approximated by a square root temporal dependence, $R_T \sim t^{1/2}$. The time instant corresponding to the switch between these two regimes reduces with increasing ambient pressure (gas density). The length of the spray at this time instant is usually associated with the breakup length of the injected jet.

4.1. Spray penetration at the early stage of injection

In Fig. 5 the tip velocity U_T is shown as a function of time t after injection. The value of this velocity is obtained by numerical differentiation of the spray length $R_T(t)$ in time. This velocity is not exactly constant, even during the first stage of the spray propagation. At ambient pressures less than 10 bar this velocity initially grows, reaches some maximum value, U_{Tmax}, and then reduces (see Fig. 5(a)).

At pressures higher than or equal to 10 bar the tip velocity reduces immediately after injection (or the characteristic time of the velocity growth is much smaller than the time step used in the experiments and thus this growth is not detected). A similar behavior is observed at other injection pressures, as shown in Fig. 5(b). The dependence of the maximum spray tip velocity on the ambient pressure is shown in Fig. 6 for different injection pressures. This maximum velocity decreases with increasing ambient pressure (increasing gas density).

The mean injection velocity is usually given in the form

$$U_i = C_d \sqrt{2\frac{p_i - p_a}{\rho}}, \tag{13}$$

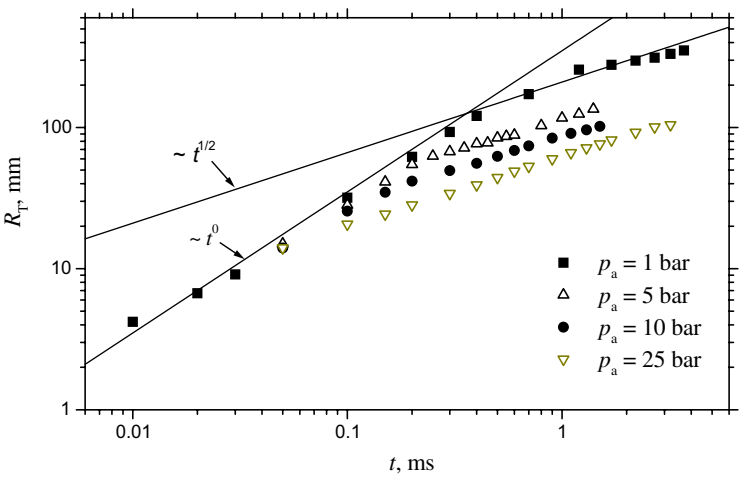

Fig. 4. Spray penetration, R_T, as a function of time at various ambient pressures p_a. The injection pressure is $p_i = 1350$ bar.

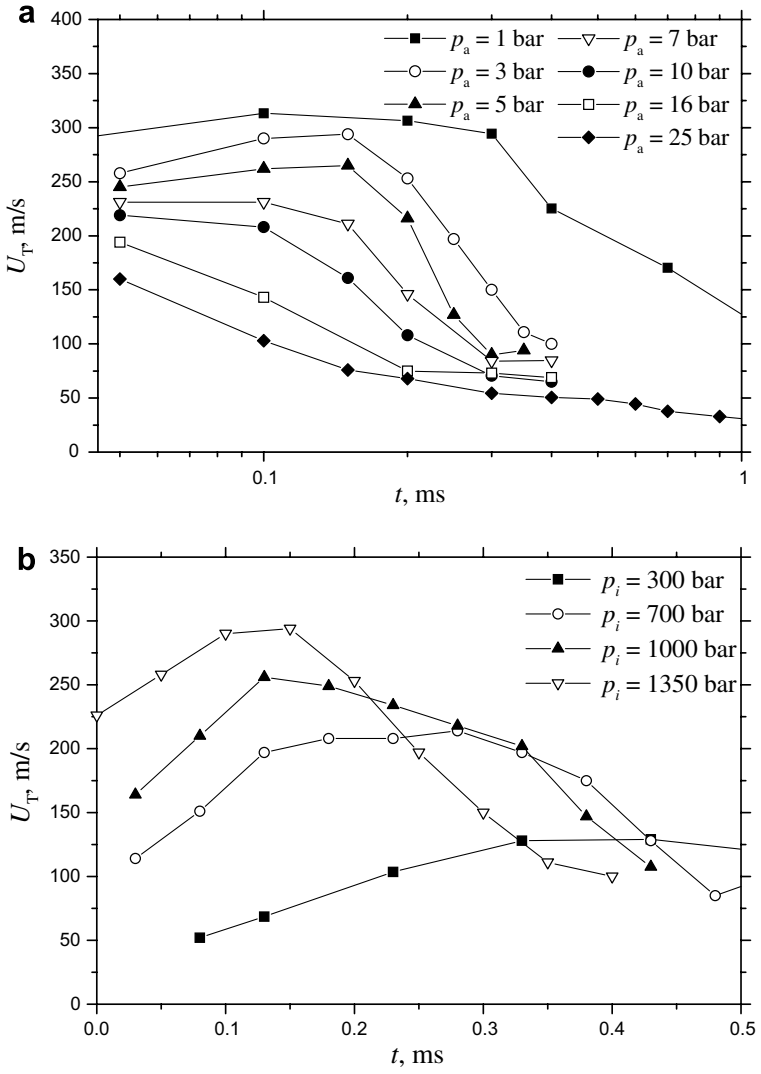

Fig. 5. The velocity of the spray tip as a function of time. (a) The injection pressure is $p_i = 1350$ bar. The ambient pressure p_a is varied from 1 bar (atmospheric pressure) to 25 bar. (b) The ambient pressure is $p_a = 3$ bar, the injection pressure is varied.

where p_i and p_a are the injection and ambient pressures, ρ is the density of the liquid fuel and C_d is a discharge coefficient associated with the pressure loss in the nozzle. For example, the lossless injection velocity ($C_d = 1$) for the conditions of Fig. 5(a) is 568 m/s. We have experimentally determined a mean injection velocity of 442 m/s for an injection pressure of 1350 bar. The mean injection velocity was determined using the measured data for the average volumetric flow rate through the nozzle. This value leads to a discharge coefficient of 0.78 for these operating conditions.

The data shown in Fig. 5(a) demonstrate that the mean injection velocity may significantly exceed the spray tip velocity, even in the initial stages of injection. Moreover, the mean injection velocity depends very little on the injection duration for the particular injector; hence the velocity is also constant over the injection duration. We conclude that the increase of spray tip velocity evident in Fig. 5(b) can be attributed to the non-stationary conditions of the ambient gas during the initial stage of injection. Moreover, the velocity growth at the times less than 0.1–0.4 ms after injection can also be explained by the pressure increase at the opening due to needle dynamics.

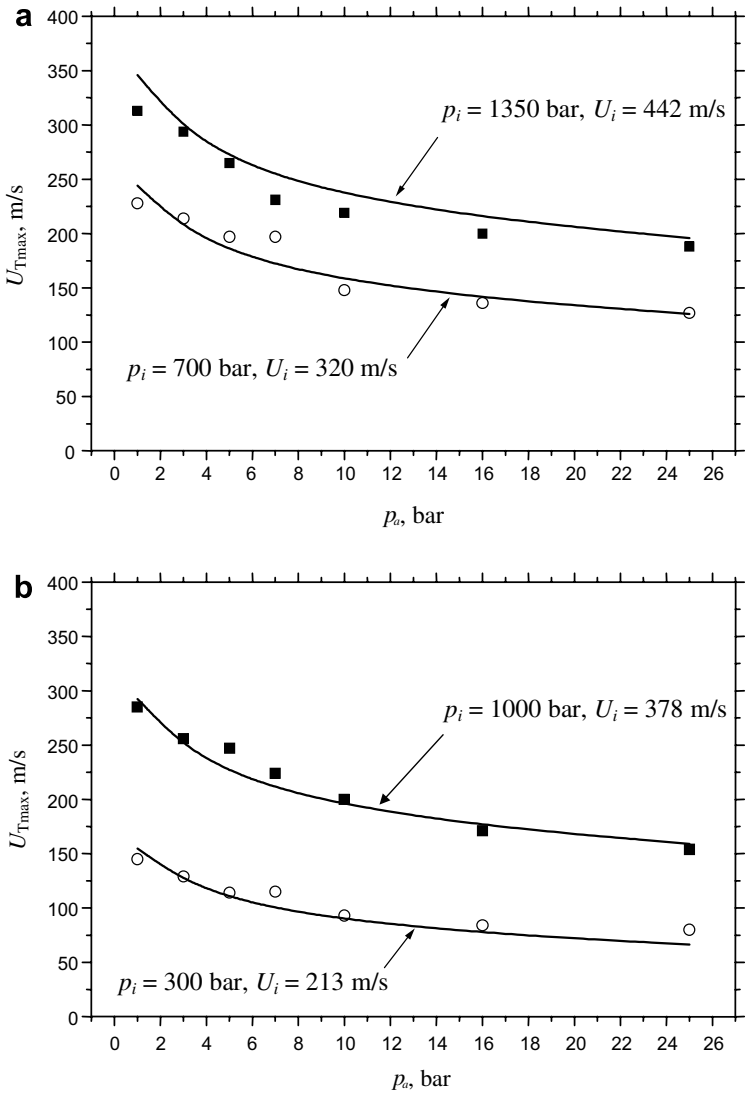

Fig. 6. Experimental data for the maximum spray-tip velocity as a function of the ambient pressure for various injection pressures. The solid lines correspond to the theoretical predictions (16).

The difference between the mean injection velocity and the spray tip velocity is accounted for by the jet deformation, atomization and by the jump conditions at the spray edge, the feature to be analytically described in the present paper.

An experimental demonstration of the complicated structure of the spray in its early stages is shown in Fig. 7. The main spray cloud in this picture follows the jet. The diameter of this jet is of order of 0.1 mm, half of the inner diameter of the nozzle. The length of this jet is approximately 1.4 times longer than the penetration length of the main spray cloud. The velocity of this jet thus approaches the value of the injection velocity. Note, that pictures including both the spray cloud and the jet are rather exceptional. Most of the images of the spray are similar to those shown in Fig. 3. In any case, the spray-tip velocity, even in the early "linear" stage, is neither equal to the injection velocity nor to the velocity of the jet tip. Note also that the drop diameter in the considered spray is of order of 5–20 μm and that the Weber number for an injection velocity $U_i = 100$ m/s is $We = \rho D U_i^2/\sigma > 1500$. Therefore the energy required for the creation of a droplet surface is negligibly small in comparison with the kinetic energy of the jet. This means that the drop velocity near the jet surface is approximately equal to the injection velocity U_i.

Fig. 7. Image of spray and liquid jet in the early stage of penetration: $p_i = 1350$ bar, $p_a = 1$ bar, $t = 0.3$ ms.

The main conclusions from the above description of the very initial stage of spray penetration are as follows. The first feature is that the spray tip velocity U_T is smaller than the injection velocity. The second feature of this stage is the increase of the spray tip velocity U_T, in spite of the fact that the mean injection velocity U_i is almost constant during injection. This fact clearly indicates that this velocity cannot be a material velocity, neither of the jet nor of the droplets.

It is shown in Fig. 4 that at some time instant, say t_B, the ''linear'' stage of spray penetration switches to the ''square-root'' stage. The velocity of the tip of the spray changes at this time instant drastically. This is the reason why the penetration length at this instant, l_B, is usually associated with the breakup length of the injected jet. In the experimental study of Arai et al. (1984), the average breakup length during injection was measured using the electric resistance method. It was shown that this measured length did not correspond well to the inferred breakup length l_B, hence it may still be useful to retain the concept of breakup length, independent of the measured length l_B.

4.2. Shock wave in the air just after injection

Consider the very initial stage of the injection. The accurate description of the initial stage of spray injection is necessary to reliably predict spray propagation at the later stages: see for example the analysis of Sazhin et al. (2003).

In our case of high-speed Diesel injection the velocity of the spray is comparable with the speed of sound c in air, but is negligibly small in comparison with the speed of sound in the liquid. Therefore, the compressibility of air must be taken into account, whereas the injected liquid fuel can be assumed to be incompressible. For sufficiently high injection velocities a shock wave develops in the air just after the injection and propagates towards the undisturbed air (see Fig. 8). Such shock waves were recently observed in the study of the fuel injection spray using X-ray technique (Degaspari, 2003). The shock wave divides the air region into an undisturbed part (ahead the shock), with the pressure and density p_a and ρ_a, and a compressible part (behind the shock), with the pressure and density p_c and ρ_c. U_i is the injection velocity of the fuel, U_{T0} is the initial tip velocity of the spray (which is the velocity of the air behind the shock), U_S is the velocity of the shock wave.

Approximating the shock as a normal adiabatic compression wave, the mass, momentum and energy balance at the wave yield (Loitsyanskii, 1966):

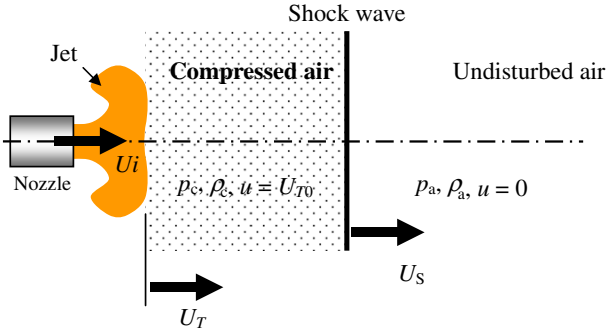

Fig. 8. Sketch of the propagating spray: the initial stage of the injection, $t < D_{Nozzle}/c$.

$$\rho_a U_S = \rho_c (U_S - U_{T0}), \quad p_a + \rho_a U_S^2 = p_c + \rho_c (U_S - U_{T0})^2, \tag{14a, b}$$

$$\frac{\kappa}{\kappa - 1}\frac{p_a}{\rho_a} + \frac{U_S^2}{2} = \frac{\kappa}{\kappa - 1}\frac{p_c}{\rho_c} + \frac{(U_S - U_{T0})^2}{2}, \tag{14c}$$

where κ is the ratio of the specific heats of the gas at constant pressure and constant volume, and the index 0 is used to denote the initial stage. The solution of Eq. (14) for the pressure in the compressed region is

$$p_c(U_{T0}) = p_a + \frac{1}{4}\left[(1+\kappa)\rho_a U_{T0}^2 + \sqrt{\rho_a} U_{T0}\sqrt{16\kappa p_a + (1+\kappa)^2 \rho_a U_{T0}^2}\right]. \tag{15}$$

The pressure p_c given by Eq. (15) defines the conditions for the shock wave, but is dependent on the spray tip velocity U_{T0}.

It should be noted that expression (15), valid for the one-dimensional geometry, is precise only for very short times, $t < D_{Nozzle}/c$. For larger times, comparable or exceeding D_{Nozzle}/c, the pressure p_c will be slightly influenced by the real geometry of the nozzle and the chamber. Therefore, expression (3) allows an estimation of the order of magnitude of the pressure p_c.

The aim of the following analysis is to predict U_{T0} from known quantities of the injection as presented in Section 2.

Already in the first images of the injected spray, when the length is approximately 5 mm, the diameter of the spray is of the order 1 mm, much larger than the nozzle diameter $D_{Nozzle} = 0.190$ mm. Noting again that the drop velocities are of order of the injection velocity U_i, the volume fraction of the liquid phase is approximately $\gamma = 0.04$. The average injection velocity U_i is obtained from the data for the volumetric flow rate through the nozzle. The pressure $p_c(U_{T0})$ at the spray tip during the initial stage of penetration is determined from (15) once the initial spray tip velocity U_{T0} is known. This velocity can be estimated by modifying Eq. (6) for the jump conditions at the initial stage

$$p_a + [\rho\gamma + \rho_a(1-\gamma)](U_0 - U_{T0})^2 = p_c(U_{T0}). \tag{16}$$

The results of the numerical solution of Eqs. (15) and (16) for the initial tip velocity U_{T0} are shown in Fig. 6 in comparison with the experimental data for the maximum spray-tip velocity. The results are rather good, indicating that the spray during the initial stage indeed consists of droplets moving with a velocity $U_0 \approx U_i$ and that the proposed jump conditions at the spray tip are appropriate. Now we can also understand why the tip velocity is not constant just after the injection, even increasing under certain conditions. On the one hand, the volume fraction of the liquid phase decreases as the spray propagates, since its cross-section increases. The decrease of γ leads to a decrease of the tip velocity. On the other hand, the initially compressed gas behind the shock wave begins to expand as the jet cross-section increases – both p_c and ρ_c decrease. We have conditions similar to an underexpanded jet issuing from a nozzle, which also exhibits initial velocity increase.

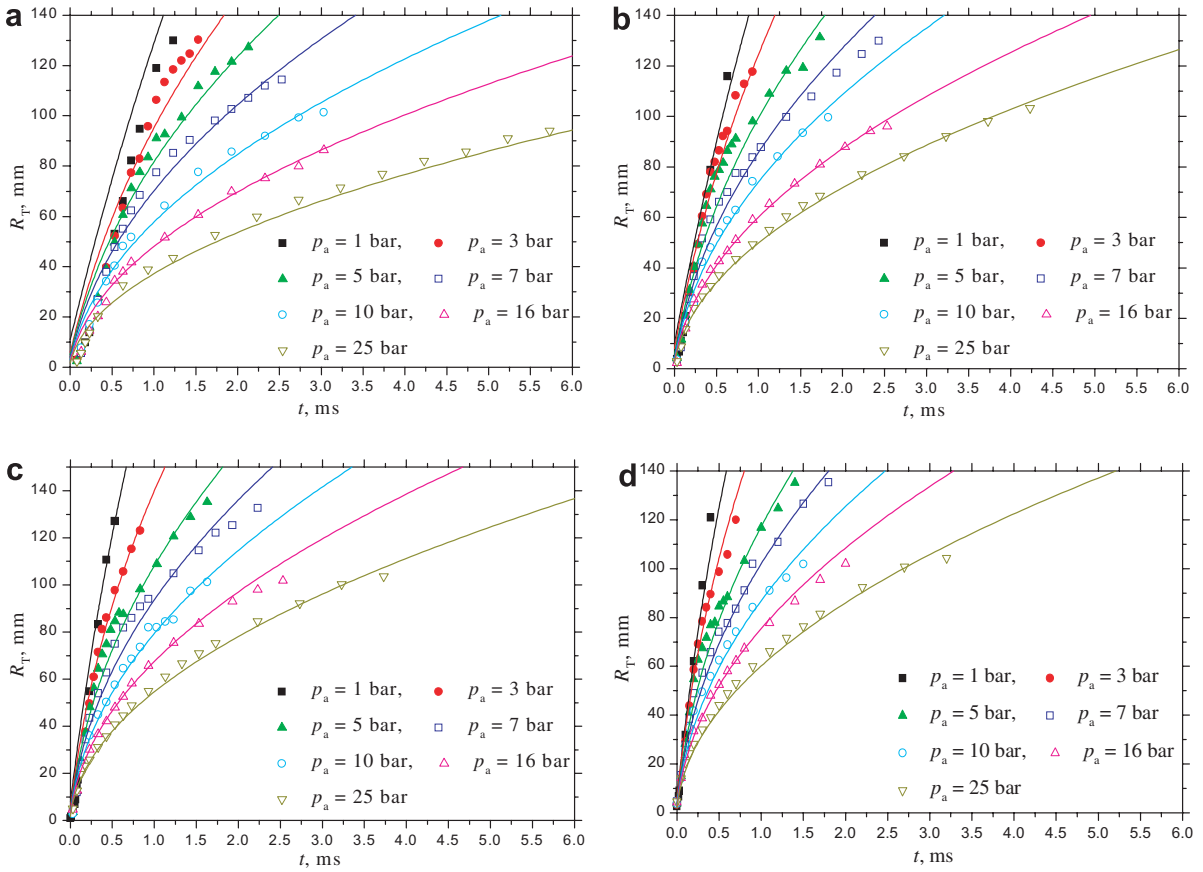

Fig. 9. Influence of the ambient pressure on the spray penetration. The injection pressures are: (a) $p_i = 300$ bar, (b) $p_i = 700$ bar, (c) $p_i = 1000$ bar, (d) $p_i = 1350$ bar. The continuous lines correspond to the proposed model.

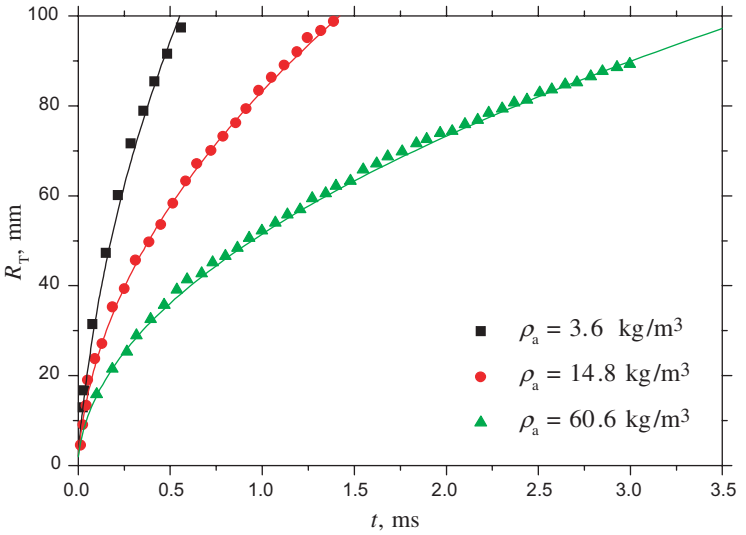

Fig. 10. Influence of the density of the ambient gas on the spray penetration. The data are from Naber et al. (1995). The continuous lines correspond to the proposed model.

4.3. Validation of the model for the far-field spray penetration

At relatively large times after injection ($t \gg D_{\mathrm{Nozzle}}/c$), the tip velocity is much smaller than the speed of sound and the spray penetration can be described using Eq. (11). A comparison of the penetration length R_{T} predicted by the proposed model with the experimental data is shown in Fig. 9. The agreement is rather good. Similar results are obtained comparing the model predictions with experimental data from the literature (see Figs. 10–12). The experimental data for the spray penetration Naber et al. (1995) in Fig. 10 is taken from the graphs in Wan and Peters (1999). In all of these comparisons, R_0, the downstream distance at which the jet breaks up, is a fitted parameter.

In Fig. 13, R_0 is shown as a function of the injection velocity and the density of the ambient gas. Fig. 13(a) shows that at low ambient pressure (1 bar), the radius R_0 decreases significantly with the injection velocity U_{i}.

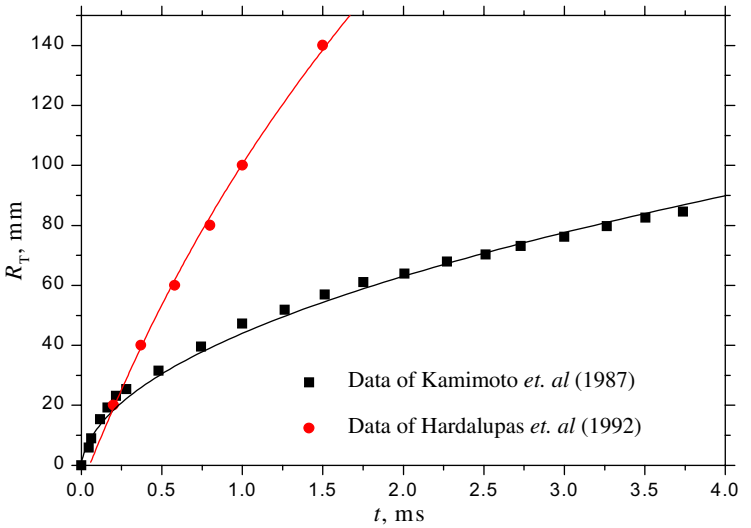

Fig. 11. Spray penetration data in comparison with the proposed model. The data are from Kamimoto et al. (1987) and Hardalupas et al. (1992).

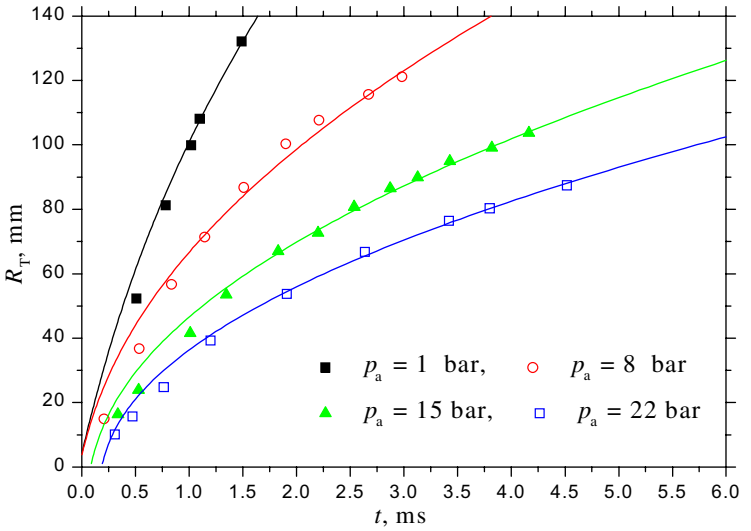

Fig. 12. Influence of the density of the ambient gas on the spray penetration. The experimental data are from Miller and Beardsley (1926). The continuous lines correspond to the proposed model.

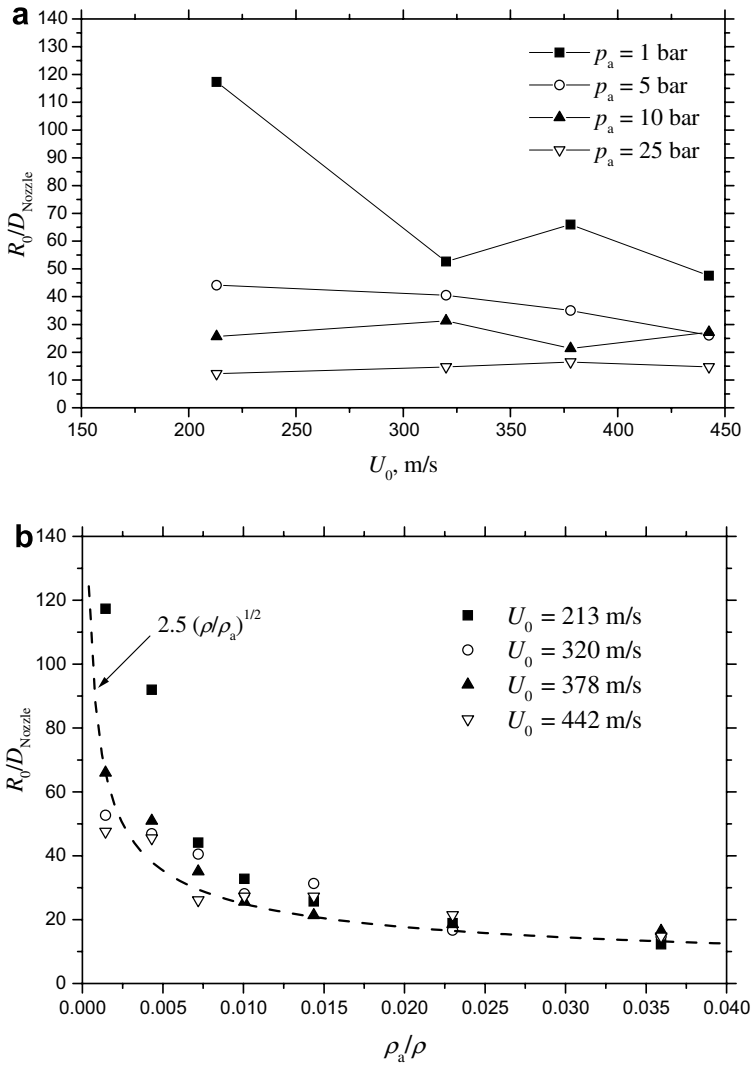

Fig. 13. Radius R_0 normalized using the inlet diameter of the nozzle: (a) as a function of injection velocity U_0; (b) as a function of the relative density of the ambient air.

This result indicates that our experiments can be associated with the "spray region", following the classification proposed in the study Arai et al. (1984).

At higher pressures the dependence of R_0 on the injection velocity U_i is not so strong. This result is in agreement with the conclusions of the study Arai et al. (1984) showing that at higher injection velocities the breakup length approaches some constant value. The breakup length reaches these constant values at a smaller velocity if the ambient pressure is higher. At these higher ambient pressures the parameter R_0 depends on the gas density (see Fig. 13(b)) and follows the square-root law obtained in Arai et al. (1984) for the breakup length for water:

$$l_B = C_B \sqrt{\frac{\rho}{\rho_a}} D, \tag{17}$$

where D is the internal diameter of the nozzle. The coefficient C_B on the right-hand side of Eq. (17) is estimated in Arai et al. (1984) to be approximately $C_B = 15.8$. Note, however, that the coefficient C_B depends partially on the geometry of the nozzle and can be different for various experimental set-ups, physical parameters of liquids and construction of nozzles.

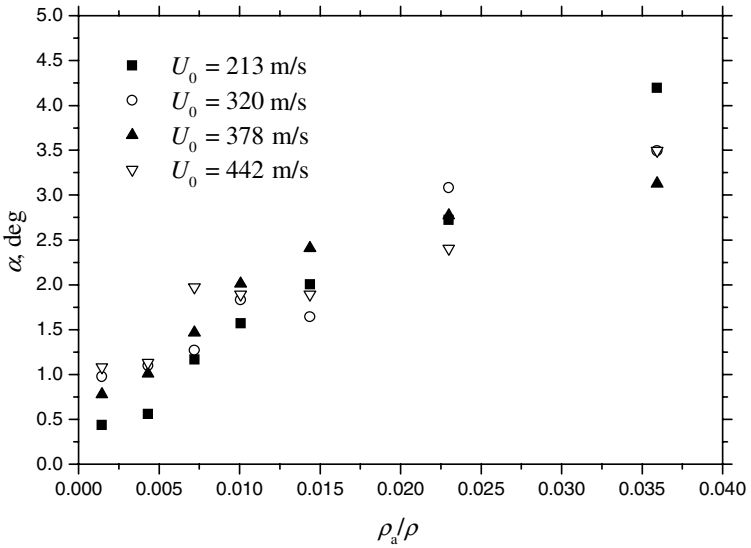

Fig. 14. Fitted value of the angle α as a function of the relative density of the ambient air.

Note that the relation (17) can serve as an indirect confirmation of our assumption that the magnitude of R_0 can be used as a scale for the breakup length of the injected Diesel jet. A more reliable confirmation can be performed only using direct measurements of the breakup length of a dense spray. This is not an easy experimental task and it is beyond the scope of the present study.

The value of the half-cone angle α obtained using Eq. (5) is shown in Fig. 14 as a function of the density ratio ρ_a/ρ. It can be seen that this angle increases monotonically with increasing ambient pressure and almost does not depend on the injection velocity. It is important to note that this angle is not exactly the half-cone angle observed on the images of spray penetration, added in Fig. 5 as α_v. These images include two main streams, the injected inner stream, whose velocity is higher than the spray tip velocity; and the outer stream influenced by the head of the spray. This second stream, whose velocity is smaller than the spray tip velocity, creates vortices near the spray-tip region. The observed spray cone angle α_v corresponds to the outer stream, whereas the angle α corresponds to the inner impinging stream.

It is not easy to estimate the values of the spray angle directly from the images of the injected spray. These values can be best evaluated analyzing the velocity profiles in the spray. Such measurements are possible using, for example, the phase Doppler instrument (Araneo and Tropea, 2000). These measurements can be the topic of an alternative study and are not considered in the present paper.

5. Conclusions

Penetration of a Diesel spray in a pressure chamber has been investigated experimentally and modeled theoretically. Penetration length and the cone angle of the spray have been measured at various injection pressures and ambient pressures.

In the proposed model for the propagation of the spray front edge two main factors are considered, namely inertia of liquid/air mixture in the steady conical region of the spray and the particular conditions near the leading edge of the spray which lead to the high gradients of the spray concentration and to the formation of the vortex-ring-like structures. These major factors determine spray penetration.

Two regions of the penetrating spray are considered in our theoretical model. One is the main region of the spray. The flow in this region is governed by the inertia of the injected liquid spray and be the momentum of the entrapped ambient air. The second considered region is the front edge of the spray. The flow of this region is governed by the inertia of the droplets entering it from the first region, as well as by the aerodynamic drag force. In the proposed model the jump conditions in this region are considered, yielding analytical expressions for the spray tip velocity and for the penetration length.

Next, accounting for the shock wave propagation in the ambient air, the model predicts the velocity of the spray tip at the initial stage of penetration.

The model for the far-field spray penetration describes the temporal dependence of the penetration length. The predictions agree well with experimental data. It was shown that the asymptotic behavior of the temporal dependence of the penetration length follows the well-known square-root law found empirically.

One fitted parameter, the breakup length R_0, is used in the model. The inverse square-root dependence of the obtained values of R_0 on the density of the ambient gas is similar to the experimental results.

References

Arai, M., Tabata, M., Hiroyasu, H., Shimizu, M., 1984. Disintegration process and spray characterization of fuel jet injected by a diesel nozzle, SAE Technical Paper 840275.

Araneo, L. and Tropea, C., 2000. Improving phase Doppler measurements in a diesel spray, SAE Technical Paper 2000-01-2047.

Birkhof, G., Macdougal, D.F., Pugh, E.M., Taylor, G.I., 1948. Explosives with lined cavities. J. Appl. Phys. 19, 563–582.

Cao, Z.-M., Nishino, K., Mizuno, S., Torii, K., 2000. PIV measurement of internal structure of diesel fuel spray. Exp. Fluids (Suppl.), S211–S219.

Cossali, G.E., 2001. An integral model for gas entrainment into full cone sprays. J. Fluid Mech. 439, 353–366.

Degaspari, J., 2003. Penetration vision, Mechanical Engineering. May 2003, pp. 60–62.

Dent, J.C., 1971. A basis for the comparison of various experimental methods for studying spray penetration, SAE Paper 710571.

Desantes, J.M., Payri, R., Salvador, F.J., Gil, A., 2006. Development and validation of a theoretical model for diesel spray penetration. Fuel 85, 910–917.

English, J., Taylor, R., Irwin, J., Mashchenko, S., 1999. An atomic Hydrogen mushroom cloud bursts out of our Galaxy, American Astronomical Soc. Meeting in Austin, Texas.

Ghosh, S., Hunt, J.C.R., 1994. Induced air velocity within droplet driven sprays. Proc. Roy. Soc. London A 444, 105–127.

Hardalupas, Y., Taylor, A.M.K.P., Whitelaw, J.W., 1992. Characteristics of the spray from a diesel injector. Int. J. Multiphase Flow 18, 159–179.

Iyer, V.A., Abraham, J., Magi, V., 2001. Exploring injected droplet size effects on steady liquid penetration in a diesel spray with a two-fluid model. Int. J. Heat Mass Trans. 45, 519–531.

Kamimoto, T., Yokota, H., Kobayashi, H., 1987. Effect of high pressure injection on soot formation processes in a rapid compression machine to simulate diesel flames, SAE Technical Paper 950279.

Kuß, D., 2000. Verhaltensstudie der Strahlausbreitung eines Common-Rail-Injektors unter dem Einfluss von Einspritz- und Umgebungsdruck in einer Hochdruck-Einspritzkammer, Student project, Technische Universtät Darmstadt, Darmstadt.

Liu, A.B., Mather D., Reitz, R.D., 1993. Modelling the effects of drop drag and breakup on fuel sprays, SAE Technical Paper 930072.

Loitsyanskii, L.G., 1966. Mechanics of Liquids and Gases. Pergamon Press, Oxford, p. 158.

Miller, H.E., Beardsley, E.G., 1926. Spray penetration with a simple fuel injection nozzle, NASA Report No. 222.

Naber, J.D., Siebers, D.L., Hencken, K.R., 1995. The Effects of high ambient density on diesel spray penetration and spread, Joint Technical Meeting 1995, Central and Western States (USA) Sections and Mexican National Section of the International Combustion Institute and American Flame Research Committee.

Naber, J.D., Siebers, D.L., 1996. Effects of gas density and vaporization on penetration and dispersion of diesel sprays, SAE Technical Papers 960034.

Pozorski, J., Sazhin, S., Waclawczyk, M., Crua, C., Kennaird, D., Heikal, M., 2002. Spray penetration in a turbulent flow. Flow, Turbul. Combust. 68, 153–165.

Roisman, I.V., Yarin, A.L., Rubin, M.B., 2001. Normal penetration of an eroding projectile into an elastic–plastic target. Int. J. Impact Eng. 25, 573–597.

Sagomonyan, A.Ya., 1974. Penetration. Moscow University Press, Moscow (in Russian).

Sazhin, S.S., Feng, G., Heikal, M.R., 2001. A model for fuel penetration. Fuel 80, 2171–2180.

Sazhin, S., Crua, C., Kennaird, D., Heikal, M., 2003. The initial stage of fuel spray penetration. Fuel 82, 875–885.

Senduka, B.A., 1998. A description of the shape of an air–fuel mixture and determination of injection advance angles related to the spark discharges in a gasoline direct inject engine, SAE Technical Paper 980496.

Sjöberg, M., 2001. The rotating injector as a tool for exploring DI diesel combustion and emissions formation processes, Doctoral Thesis, Royal Institute of Technology, Sweden.

di Stasio, S., Valentino, G., Corcione, F.E., 2000. Spray boundary concept and droplet size distribution of dense diesel jets by different laser experiments. In: Proceedings 16th Annual Conference on Liquid Atomization and Spray Systems, ILASS Europe-2000, pp. I.15.1–I.15.6.

Staufer, D., 1979. Scaling theory of percolation clusters. Phys. Rep. 54, 1–74.

Staufer, D., 1985. Introduction to Percolation Theory. Taylor & Francis, London.

Stegemann, J., Seebode, J., Baltes, J., Baumgarten, C., Merker, G.P., 2002. Influence of throttle effects at the needle seat on the spray characteristics of a multihole injection nozzle. In: Proceedings of the 18th Annual Conference on Liquid Atomization and Spray Systems, ILASS Europe-2002.

Wan, Y., Peters, N., 1999. Scaling of spray penetration with evaporation. Atomizat. Sprays 9, 111–132.

Yarin, A.L., 1993. Free Liquid Jets and Films: Hydrodynamics and Rheology. Longman & Wiley, New York.